

# On the strong impact of doping in the triangular antiferromagnet $\text{CuCrO}_2$

Antoine Maignan,<sup>1</sup> Christine Martin,<sup>1</sup> Raymond Frésard,<sup>1</sup> Volker Eyert,<sup>1,2</sup>  
Emmanuel Guilmeau,<sup>1</sup> Sylvie Hébert,<sup>1</sup> Maria Poienar,<sup>1</sup> and Denis Pelloquin<sup>1</sup>

<sup>1</sup>Laboratoire CRISMAT, UMR CNRS-ENSICAEN(ISMRA) 6508, and IRMA, FR3095, Caen, France

<sup>2</sup>Center for Electronic Correlations and Magnetism,

Institut für Physik, Universität Augsburg, 86135 Augsburg, Germany

(Dated: October 27, 2018)

Electronic band structure calculations using the augmented spherical wave method have been performed for  $\text{CuCrO}_2$ . For this antiferromagnetic ( $T_N = 24$  K) semiconductor crystallizing in the delafossite structure, it is found that the valence band maximum is mainly due to the  $t_{2g}$  orbitals of  $\text{Cr}^{3+}$  and that spin polarization is predicted with  $3 \mu_B$  per  $\text{Cr}^{3+}$ . The structural characterizations of  $\text{CuCr}_{1-x}\text{Mg}_x\text{O}_2$  reveal a very limited range of  $\text{Mg}^{2+}$  substitution for  $\text{Cr}^{3+}$  in this series. As soon as  $x = 0.02$ , a maximum of 1% Cr ions substituted by Mg site is measured in the sample. This result is also consistent with the detection of Mg spinel impurities from X-ray diffraction for  $x = 0.01$ . This explains the saturation of the  $\text{Mg}^{2+}$  effect upon the electrical resistivity and thermoelectric power observed for  $x > 0.01$ . Such a very weak solubility limit could also be responsible for the discrepancies found in the literature. Furthermore, the measurements made under magnetic field (magnetic susceptibility, electrical resistivity and Seebeck coefficient) support that the  $\text{Cr}^{4+}$  "holes", created by the  $\text{Mg}^{2+}$  substitution, in the matrix of high spin  $\text{Cr}^{3+}$  ( $S = 3/2$ ) are responsible for the transport properties of these compounds.

PACS numbers: 71.20.-b, 72.20.Pa, 72.25.-b

Keywords:

## I. INTRODUCTION

Because of their remarkable properties, layered oxides with mixed-valent transition-metal atoms have attracted much attention in the last twenty years. After the discovery of the high- $T_c$  superconducting cuprates [1] with two-dimensional (2D) structures, in which perovskite  $[\text{ACuO}_{3-\delta}]_\infty$  layers are sandwiched in between layers acting as charge reservoirs, the layered cobaltites based on  $\text{CoO}_2$  layers with the  $\text{CdI}_2$  structure have been more recently deeply investigated. Apart from the cationic conduction in  $\text{Li}_x\text{CoO}_2$ , an effective battery material [2], the analogous compound  $\text{Na}_x\text{CoO}_2$  has been shown to exhibit promising thermoelectric properties for  $x \sim 0.5$  [3] whereas the hydrated form of  $\text{Na}_{0.3}\text{CoO}_2$  exhibits superconductivity [4]. From the structural point of view, the  $\text{CoO}_2$  layers can be described as planes of edge sharing  $\text{CoO}_6$  octahedra forming a 2D triangular cobalt lattice [5]. This triangular network is responsible for the frustrated magnetism. The particular rhombohedral splitting of the cobalt  $t_{2g}$  orbitals has been invoked to explain the coexistence of two subbands,  $a_{1g}$  and  $e'_g$ , narrow and broad, respectively, the former being responsible for the large Seebeck coefficient whereas the metallic behaviour is associated with the latter [6].

In this context, the coexistence of complex magnetic structure [7] and ferroelectricity [8] in the delafossite structure  $\text{CuFeO}_2$  is very interesting. In this compound crystallizing in the  $R\bar{3}m$  space group, the  $\text{FeO}_6$  octahedra layers are isostructural to the  $\text{CoO}_6$  layer of the  $\text{Na}_x\text{CoO}_2$  system [9]. The main difference lies in the separating layer with a linear coordination of monovalent copper, since the O-Cu-O bridges ensure the connec-

tion between successive  $\text{FeO}_2$  planes. The presence of high spin ( $S = 5/2$ ) at the B-site of the  $\text{AFeO}_2$  delafossite together with the triangular spin frustration creates complex antiferromagnetic states, coupled to structural transitions, with modulations of the magnetic structure linked to ferroelectricity [8,10]. However, the very stable high spin configuration of  $\text{Fe}^{3+}$ , precluding the possibility to induce electrical conductivity, is in marked contrast with the low electrical resistivity reported for the chromium based analogous delafossite,  $\text{CuCr}_{1-x}\text{Mg}_x\text{O}_2$  [11,12]. The  $\text{CuCrO}_2$  compound is clearly insulating and its magnetic structure, established by neutron diffraction data refinements, revealed a complex antiferromagnetic incommensurate structure with a short magnetic correlation length along  $c$  and a maximal magnetic moment of  $\sim 3\mu_B$  [13,14]. Clear evidence for magnetic ordering below  $T_N$  is provided by specific heat measurements as well, for both undoped and Mg-doped samples [11], the former being also a multiferroic [15]. However, the electrical resistivity drop induced by the  $\text{Mg}^{2+}$  for  $\text{Cr}^{3+}$  substitution and its relation to the structural properties has not yet been clearly elucidated. The values of the transport coefficients show discrepancies, too. Indeed, according to Ono et al. [12], the resistivity of  $\text{CuCr}_{0.98}\text{Mg}_{0.02}\text{O}_2$  at room temperature (RT) is about  $1 \Omega \text{ cm}$ , while according to Okuda et al. it is rather one order of magnitude smaller [11]. Regarding the thermopower at room temperature, the former authors reported a value around  $280 \mu\text{V/K}$  whereas the latter obtained  $100 \mu\text{V/K}$ . Besides, some authors mentioned a hole creation at the A site by charge compensation,  $\text{Cu}_{1-x}^+\text{Cu}_x^{2+}\text{Cr}_{1-x}^{3+}\text{Mg}_x^{2+}\text{O}_2$  [11], whereas others considered a mixed valency  $\text{Cr}^{3+}/\text{Cr}^{4+}$  according to  $\text{Cu}^+\text{Cr}_{1-2x}^{3+}\text{Cr}_x^{4+}\text{Mg}_x^{2+}\text{O}_2$  [12]. For all these

reasons the  $\text{CuCr}_{1-x}\text{Mg}_x\text{O}_2$  system has been revisited.

In the present paper, we report on electronic band structure calculations for the undoped compound  $\text{CuCrO}_2$  and on a complete experimental study of the series  $\text{CuCr}_{1-x}\text{Mg}_x\text{O}_2$ . Special care has been taken with the chemistry problem of the solubility of  $\text{Mg}^{2+}$  at the chromium site.

## II. METHODOLOGY

### A. Electronic structure calculations: Theoretical method

The electronic band structure calculations were based on density-functional theory and the generalized gradient approximation (GGA) [16] with the local-density approximation parameterized according to Perdew and Wang [17]. They were performed using the scalar-relativistic implementation of the augmented spherical wave (ASW) method (see Refs. [18,19,20] and references therein). In the ASW method, the wave function is expanded in atom-centered augmented spherical waves, which are Hankel functions and numerical solutions of Schrödinger's equation, respectively, outside and inside the so-called augmentation spheres. In order to optimize the basis set, additional augmented spherical waves were placed at carefully selected interstitial sites. The choice of these sites as well as the augmentation radii were automatically determined using the sphere-geometry optimization algorithm [21]. Self-consistency was achieved by a highly efficient algorithm for convergence acceleration [22]. The Brillouin zone integrations were performed using the linear tetrahedron method with up to 1313  $\mathbf{k}$ -points within the irreducible wedge of the rhombohedral Brillouin zone [20,23].

In the present work, a new full-potential version of the ASW method was employed [24]. In this version, the electron density and related quantities are given by spherical harmonics expansions inside the muffin-tin spheres. In the remaining interstitial region, a representation in terms of atom-centered Hankel functions is used [25]. However, in contrast to previous related implementations, we here get away without needing a so-called multiple- $\kappa$  basis set, which fact allows us to investigate rather large systems with a minimal effort.

### B. Sample preparation and characterization

Polycrystalline samples of  $\text{CuCr}_{1-x}\text{Mg}_x\text{O}_2$ , ( $0 \leq x \leq 0.08$ ) have been prepared by solid-state reaction by mixing  $\text{Cu}_2\text{O}$ ,  $\text{Cr}_2\text{O}_3$  and  $\text{MgO}$  within the stoichiometric ratios  $0.5:0.5(1-x):x$ . The powders were then pressed into bars and fired at  $1200^\circ\text{C}$  for 12 h in air.

As explained in the following, due to the observation of impurities for low Mg level, to study the possibility of holes created by a lack of  $\text{Mg}^{2+}$  for  $\text{Cr}^{3+}$  substitution, i.e.

vacancies at the Cu or Cr sites, two samples,  $\text{Cu}_{0.98}\text{CrO}_2$  and  $\text{CuCr}_{0.98}\text{O}_2$ , were also prepared in the same conditions. A third sample of formula  $\text{Cu}_{1.02}\text{Cr}_{0.98}\text{O}_2$  was also made to force a Cu substitution for Cr, i.e. to induce tetravalent chromium if the oxidation of Cu is less than three. Additionally, as hole creation can result from an oxygen excess, two samples with different nominal oxygen contents,  $\text{CuCrO}_2$  and  $\text{CuCrO}_{2.5}$ , obtained by mixing the precursors  $\text{Cu}_2\text{O}$  or  $\text{CuO}$  and  $\text{Cr}_2\text{O}_3$ , were also prepared by firing, at the same temperature, the bars in silica tubes sealed under primary vacuum. To also check for oxygenation non-equilibrium phenomena, these samples were either cooled by quenching in air from  $1200^\circ\text{C}$  or by cooling at  $100^\circ\text{C/h}$  and  $50^\circ\text{C/h}$ .

The quality of the obtained bars was systematically checked by X-ray powder diffraction (XRPD) data collected by using a PANalytical X'pert Pro diffractometer ( $\text{Cu } K_\alpha$ ,  $12^\circ \leq 2\theta \leq 112^\circ$ ). A Zeiss SUPRA 55 scanning electron microscope was also used to observe the microstructure of the samples. The cationic compositions were checked by an EDAX energy dispersive X-ray spectroscopy (EDS) system. Transmission electron microscopy analyses were also carried out with a JEOL 2010CX microscope equipped with an EDS INCA analyser. It must be emphasized that the low level of magnesium content to be detected is at the limit of the analyser. The sample preparation for these observations was made by crushing in butanol small pieces of bars and the corresponding microcrystals were deposited on Ni grids. On the EDS spectrum, in addition to the characteristic peaks of the Cu, Cr and Mg elements, peaks of Ti, C and Ni were also observed, due to the sample holder and Ni grid.

The resistivity ( $\rho$ ) measurements were made by the four-probe technique using ultrasonically deposited indium contacts. The temperature or magnetic field dependent data were collected by using a Quantum Design physical properties measurement system (PPMS) equipped with superconducting coils delivering maximum fields of 7 T or 9 T with temperatures up to 400 K. A steady-state technique was used in a similar set-up in order to measure the Seebeck coefficient (S) with a typical gradient of  $T = 1$  K. The  $\rho$  and S data were collected upon cooling from 400 K and 315 K, respectively. An Ulvac-Zem3 set-up was also used to extend the resistivity measurements to higher temperatures (T maximum of 1073 K). The magnetic susceptibility was obtained by dividing the magnetization (M) by the magnetic field (0.3 T) with M data collected in zero-field cooling mode by using a SQUID magnetometer (MPMS, Quantum Design, maximum magnetic field of 5 T).

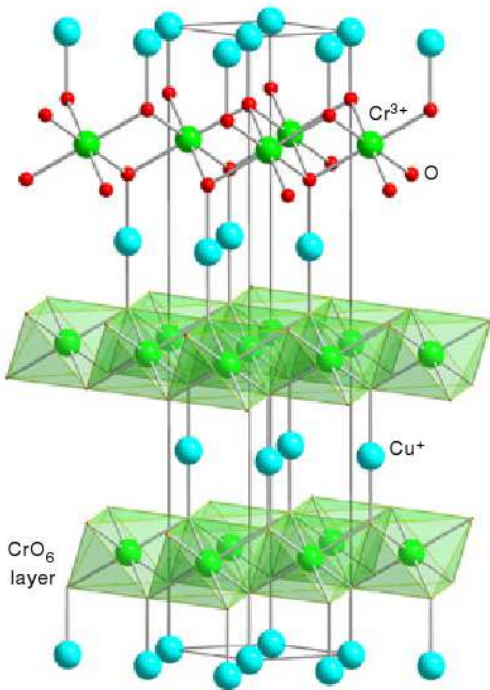


FIG. 1: Crystal structure of CuCrO<sub>2</sub>. Copper, chromium and oxygen atoms are shown as spheres, blue, green and red, respectively. The connection between two successive layers of CrO<sub>6</sub> octahedra is made through O-Cu-O dumbbells.

### III. RESULTS

#### A. Electronic structure calculations for CuCrO<sub>2</sub> : Results and discussion

The calculations used the crystal structure data reported by Crottaz et al. [26], and depicted in Fig. 1. As a starting point, spin-degenerate calculations for the rhombohedral structure were performed. In the resulting partial densities of states (DOS) the lower part of the spectrum is dominated by O 2*p* states and the transition metal d states lead to rather sharp peaks in the interval from -4 to +3 eV. In particular, one obtains the *t*<sub>2*g*</sub> and *e*<sub>g</sub> manifolds of the Cr 3*d* states as resulting from the octahedral coordination. This representation of the partial DOS refers to a local rotated coordinate system with the Cartesian axes pointing towards the oxygen atoms.  $\sigma$ -type overlap of the O 2*p* states with the Cr 3*d e*<sub>g</sub> orbitals leads to the contribution of the latter between -7 and -6 eV. In contrast, due to the much weaker  $\pi$ -type overlap of the O 2*p* states with the *t*<sub>2*g*</sub> orbitals, these states give rise to sharp peaks in the interval from -1.0 to 0.3 eV. The Fermi energy falls into the middle of the *t*<sub>2*g*</sub> manifold and gives rise to a *d*<sup>3</sup> state. From this and the fact that  $E_F$  is very close to the highest peak we would expect long-range ferromagnetic ordering of Cr moments of 3  $\mu_B$  in a spin-polarized calculation. This result is compatible with the scenario used in the cobaltites in which

the *t*<sub>2*g*</sub> orbitals splitted by the rhombohedral distortion are responsible for the large values of the Seebeck coefficient [6]. The Cu 3*d* states are essentially limited to the interval from -4 to -1 eV and thus Cu can be assigned a monovalent d10 configuration in close analogy with the experimental findings.

While previous studies reported a possible 120° magnetic structure [13], more recent neutron diffraction experiments confirm that the magnetic structure is far more complex [14]. In view of this still unsettled situation, we opted to perform subsequent spin-polarized calculations for an assumed ferromagnetic state in the same manner as in the previous work by Galakhov et al., by Ong et al., and by ourselves on CuFeO<sub>2</sub> [27,28,29]. In contrast to the title compound this material does not show long-range antiferromagnetic order in the ideal rhombohedral structure. Yet, as has been pointed out by Ye et al., CuFeO<sub>2</sub> undergoes several structural distortions and assumes a monoclinic structure with space group C2/m at 4 K [10]. The latter allows for an antiferromagnetically ordered ground state as has been confirmed by our calculations [29]. While performing this study on CuFeO<sub>2</sub>, we were able to show that the electronic states calculated for the antiferromagnetic ground state and an assumed ferromagnet are very similar apart from the fact that the former displays a finite optical band gap. Actually, this striking similarity was just a consequence of the strongly localized nature of the Fe 3*d t*<sub>2*g*</sub> states. To conclude, using an assumed ferromagnetic state for investigating the electronic properties of the title compound is well justified as long as we are interested in the electronic properties.

From these calculations, a stable ferromagnetic configuration was obtained with magnetic moments of 3.0  $\mu_B$ . Most importantly, the density of states as displayed in Fig. 2 reveals the opening of a fundamental band gap of about 1.2 eV between the spin-up and spin-down Cr 3*d t*<sub>2*g*</sub> states, which also carry the overwhelming part of the

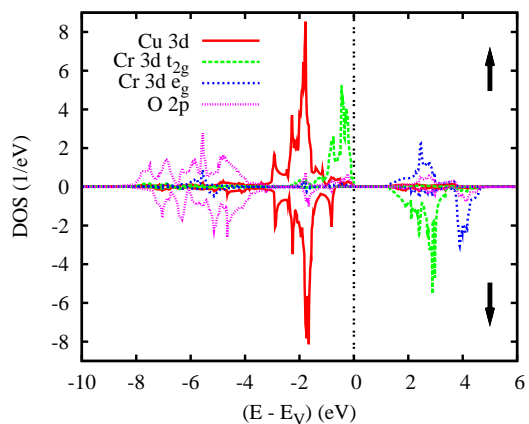


FIG. 2: Partial densities of states (DOS) of rhombohedral CuCrO<sub>2</sub>.

magnetic moment. In contrast, the polarization of O  $2p$  states is rather low as is expected from the small overlap with the  $t_{2g}$  states (see Ref. [29,30] for a more detailed discussion). In passing, we mention that according to the above-mentioned results for  $\text{CuFeO}_2$  we expect very similar electronic states from spin-polarized calculations using long-range antiferromagnetic order. In particular, due to its reduced symmetry, such a state is very likely to also display insulating behaviour.

The electronic bands along selected high-symmetry lines of the first Brillouin zone of the hexagonal lattice, Fig. 3, are displayed in Fig. 4. Clearly their dispersion

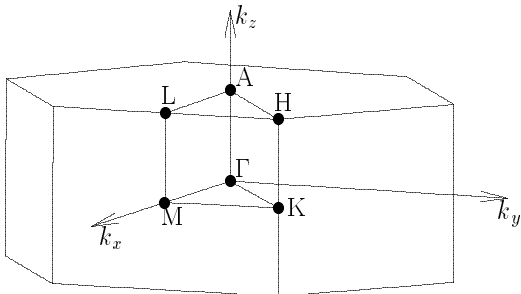


FIG. 3: First Brillouin zone of the hexagonal lattice.

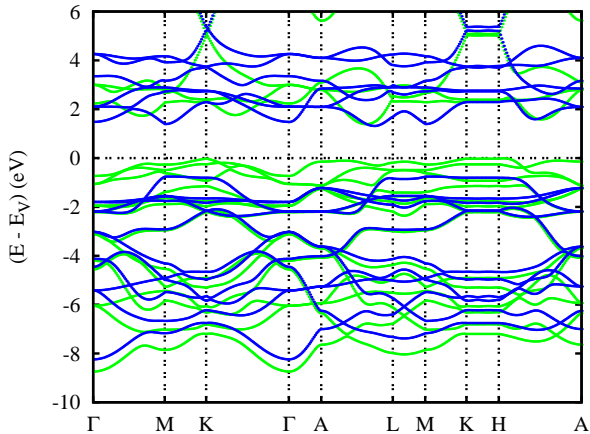


FIG. 4: Electronic bands of rhombohedral ferromagnetic  $\text{CuCrO}_2$ . Green (blue) curves correspond to the majority (minority) spin bands.

in the vicinity of the Fermi energy exhibits an intricate behaviour. First, the dispersion is quite substantial in most directions, pointing towards a considerable three-dimensionality of the electronic states arising from the coupling between the layers as has been observed also in other delafossite materials [29,30,31]. In particular, its magnitudes along  $\Gamma$ -K and  $\Gamma$ -A are very similar. Second, we obtain that two bands are reaching the Fermi energy, both at the K and the H point. Nevertheless their dispersion along K-H (and M-L) is much smaller than along the  $\Gamma$ -A direction.

These calculations allow drawing a number of conclusions. First of all, the dispersion of the highest occupied bands is remarkably small, as can be seen from the bands around the H and K points. Accordingly, assuming a vanishingly small hole doping, one expects a natural tendency towards localization of the low-energy excitations, even without strong correlations. Besides, including the latter is expected to enhance this tendency towards localization. The localized character of these excitations may even result in a structural transition, as happens in, for example, the related compound  $\text{CuFeO}_2$  [10], where the distorted structure is further stabilized by superexchange processes [29]. In  $\text{CuCrO}_2$ , the situation appears less extreme, as no structural distortion is observed. This may be due to the fact that the spin carried by the  $\text{Cr}^{3+}$  ions is smaller than the one carried by the  $\text{Fe}^{3+}$  ions. In that case the amount of superexchange energy that is lost due to frustration is reduced, and there is no need for the system to distort in order to recover that energy.

Finally, in a rigid band picture, one can anticipate that hole doping should result in peculiar effects. For very small doping, even though the Fermi velocity increases, it remains small. In such a case, the formation of small polarons is expected and the system should remain insulating while mostly keeping the magnetic structure of the undoped compound. Under further doping the resulting increase of the Fermi velocity should result in a more metallic behaviour, accompanied by spin dependent transport.

In order to check these predictions, we performed a series of susceptibility and transport measurements on weakly Mg-doped  $\text{CuCrO}_2$  samples.

## B. Structural study

The X-ray powder diffraction study of the  $\text{CuCr}_{1-x}\text{Mg}_x\text{O}_2$  compounds prepared in air reveals a very limited  $\text{Mg}^{2+}$  solubility range, as shown by the patterns in Fig. 5. In addition to the main diffraction peaks coming from the  $R\bar{3}m$  delafossite phase (with  $a \simeq 2.97$  and  $c \simeq 17.10$  Å in the hexagonal setting), extra peaks (indicated by black arrows in Fig. 5) corresponding to the  $Fd\bar{3}m$  space group with  $a \simeq 8.33$  Å and thus attributed to  $\text{MgCr}_2\text{O}_4$  can be detected as soon as  $x \simeq 0.01$ . Furthermore, the presence of a second impurity phase, identified as  $\text{CuO}$ , is also observed for the compounds corresponding to  $x = 0.04$  and  $0.05$ . This preliminary analysis is consistent with the observations made by scanning electron microscopy. As shown in Fig. 6 for  $\text{CuCr}_{0.99}\text{Mg}_{0.01}\text{O}_2$ , the material is composed mainly of large plate-like grains (the EDS analysis of which leads to a Cu/Cr ratio close to 1) and of smaller grains of octahedral shape, corresponding to the spinel phase (in agreement with the EDS results: Mg/Cr = 0.5).

At first glance, these results point towards an apparent lack of  $\text{Mg}^{2+}$  solubility or a very limited solubility



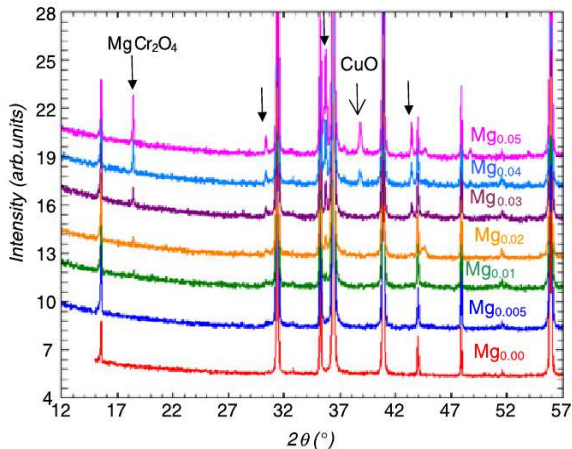


FIG. 5: Enlargement of the low-angle part of the X-ray diffraction patterns of the  $\text{CuCr}_{1-x}\text{Mg}_x\text{O}_2$  ( $x = 0.005, 0.01, 0.02, 0.03, 0.04, 0.05$ ) samples characteristic of the delafossite phase.  $\downarrow$  and  $\downarrow$  indicate peaks attributed to the  $\text{MgCr}_2\text{O}_4$  spinel and  $\text{CuO}$  that appear as impurities.

range. However, as shown in the next section, by RT measurement of the Seebeck coefficient  $S$ , which is a sensitive probe of the charge carrier concentration, positive  $S$  values for all  $x$  are found with a magnitude that decreases as  $x$  increases up to  $x \simeq 0.02$ . This indicates an increase of the hole concentration in the nominal  $\text{CuCr}_{1-x}\text{Mg}_x\text{O}_2$  formula. By combining these results – in agreement with previous reports – with the study of the X-ray patterns showing the presence of impurities as soon as  $\text{CuCr}_{0.99}\text{Mg}_{0.01}\text{O}_2$ , it appears that in addition to the Mg substitution, non-stoichiometry phenomena could also be responsible for creating holes in  $\text{CuCrO}_2$ . In order to address this crucial problem, several additional experiments were made as aforementioned in Section II B. The  $S$  values were measured at 300 K for all samples. For all samples without magnesium (with cation deficiencies or excess oxygen and also for the sample with  $\text{Cu}/\text{Cr} > 1$ ) prepared at the same conditions as  $\text{CuCr}_{1-x}\text{Mg}_x\text{O}_2$  no significant  $S$  change compared to  $\text{CuCrO}_2$  could be evidenced, with all  $S$  values at 300 K lying near  $S \simeq 1\text{mV}/\text{K}$ . These compounds were also post-annealed under oxygen at 100 atm ( $600^\circ\text{C}$ , 12 h) but without significant effect on the transport properties. Thus our results show that the oxygen content does not change significantly in those delafossite samples. This is confirmed by an independent neutron powder diffraction study of air-prepared polycrystalline samples of  $\text{CuCrO}_2$  and  $\text{CuCr}_{0.98}\text{Mg}_{0.02}\text{O}_2$  ( $x = 0.02$ ) which confirms their  $\text{O}_2$  stoichiometry (in the accuracy of the technique) [14]. All the corresponding  $S_{300\text{K}}$  values are close to  $\sim 1\text{mV}/\text{K}$  for the Mg-free samples. Such a value is similar to the one reported in Ref. [12] but much higher than that of Ref. [11]. This strongly suggests that the samples in Ref. [11] have chemical formulas different from the nominal compositions.

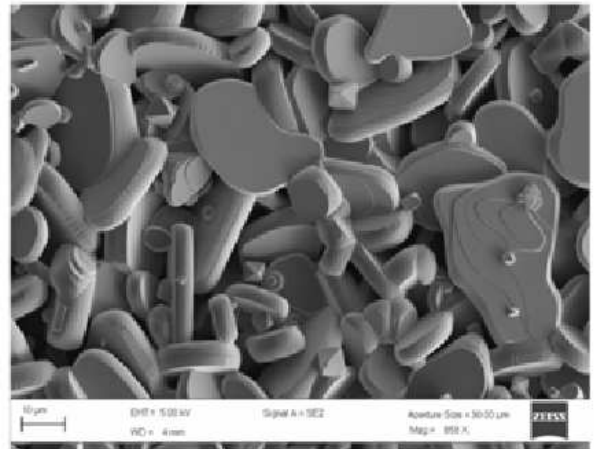


FIG. 6: SEM image of  $\text{CuCr}_{0.99}\text{Mg}_{0.01}\text{O}_2$ . The largest platelet-like microcrystals correspond to the delafossite phase whereas the small crystals of octahedral shape are attributed to spinel impurity.

Finally, the Mg presence in the delafossite micrograins was demonstrated by using EDS analysis coupled to electron diffraction in the transmission electron microscope for the air-prepared  $\text{CuCr}_{0.98}\text{Mg}_{0.02}\text{O}_2$  sample. As shown in Fig. 6, the analyzed regions were chosen on the basis of their electron diffraction (ED) patterns characteristic of the delafossite structure ( $c$ -axis parameter of  $\simeq 17\text{Å}$  compatible with the  $R\bar{3}m$  space group of the delafossite). The EDS analysis statistics made on 10 microcrystals leads to an average measured Mg content  $x_{\text{mes.}} \simeq 0.01$ . Although the proof of the Mg substitution in  $\text{CuCrO}_2$  is established, its low concentration makes very difficult a quantitative determination. This very limited substitution range of about 1% to be compared to the nominal content of 2% could be explained by the poor adaptability of the compact  $\text{MO}_2$  layers in this structural type. The larger  $\text{Mg}^{2+}$  ionic radius than that of  $\text{Cr}^{3+}$ ,  $r_{\text{Cr}^{3+}} = 0.0615\text{nm}$  against  $r_{\text{Mg}^{2+}} = 0.072\text{nm}$ , could be the reason for the limited range of Mg substitution.

In order to compare the structural parameters to those reported in previous studies [11], the X-ray data of the present samples were also refined in the delafossite structure ( $R\bar{3}m$ , space group). According to the unit cell parameters and volumes given in Fig. 7, the changes are small but beyond the error of the technique, with  $(a_0 - a_{0.04})/a_0 = -0.03\%$  and  $(c_0 - c_{0.04})/c_0 = 0.06\%$ , i.e. clearly smaller than what is reported in Ref. [11] (0.3% and 0.2%, respectively). Moreover, plateaus in the  $a$  (or  $c$ ) =  $f(x)$  curves are observed for  $x \geq 0.03$  which also differ from the monotonic evolution reported in Ref. [11]. Finally, it is found that the unit cell volume remains almost constant as  $x$  increases (in the range  $131.08\text{Å}^3 - 131.11\text{Å}^3$ ), which is consistent with the limited magnesium solubility (inset of Fig. 7).

In conclusion of this structural part, it is found that the Mg substitution is limited to about  $\sim 1\%$ . This maxi-

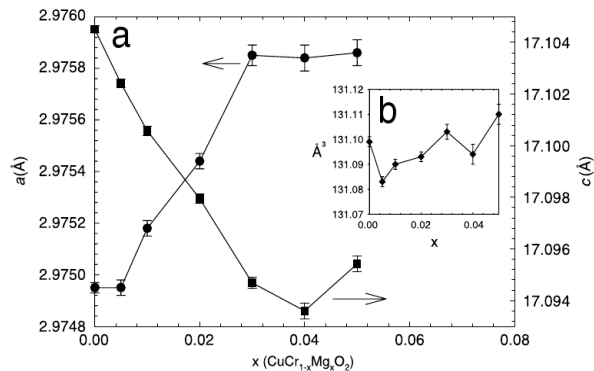


FIG. 7: Main panel (a) Unit cell parameters (a: circles, left y-axis ; c: squares, right y-axis) as a function of the nominal  $\text{Mg}^{2+}$  content  $x$  in  $\text{CuCr}_{1-x}\text{Mg}_x\text{O}_2$ . Inset (b)  $x$  dependence of the corresponding unit cell volume.

imum is obtained as soon as  $x = 0.02$  in  $\text{CuCr}_{1-x}\text{Mg}_x\text{O}_2$ . It must be emphasized that this very low solubility is lower than previously reported in Ref. [11,12]. This very low amount of substitution also explains the limited variation of the unit cell parameters with the substitution. Remarkably, this small amount is sufficient to strongly affect the transport properties. However, one cannot exclude that this substitution is also accompanied by other hardly measurable non-stoichiometry phenomena such as changes in the Cu/Cr ratio and/or the oxygen content. But what is clear is the appearance of the  $\text{MgCr}_2\text{O}_4$  spinel impurity.

### C. Physical measurements

At first glance, it is difficult to relate the structural results to the strong impact induced by the  $\text{Mg}^{2+}$  substitution on the magnetic susceptibility  $\chi$  (Fig. 8), electrical resistivity  $\rho$  (Fig. 9) and Seebeck coefficient  $S$  (Fig. 10). First, it must be pointed out that the  $\text{CuCrO}_2$  sample with  $\rho_{300\text{ K}} = 1\text{ k}\Omega\text{ cm}$ ,  $S_{300\text{ K}} = 1.1\text{ mV/K}$  appears to be less self-doped than in the previous study of Ref. [11] ( $\rho_{300\text{ K}} = 0.2\text{ k}\Omega\text{ cm}$ ,  $S_{300\text{ K}} = 0.35\text{ mV/K}$ ). Second, the  $\chi(T)$  curve of  $\text{CuCrO}_2$  reveals a characteristic downturn below  $\sim 24\text{ K}$  (Fig. 8) which is in good agreement with the value  $T_N = 24\text{ K}$  reported in the literature for  $\text{CuCrO}_2$  [11,13,14]. More importantly, the  $\chi$  values just above  $T_N$  are smaller than those of the  $\text{Mg}^{2+}$  substituted  $\text{CuCrO}_2$  compounds (Fig. 8). This is also clearly seen as well-defined  $\chi(T)$  peaks at  $T_N \sim 25\text{ K}$  observed for the doped compounds compared to a smoother maximum for  $\text{CuCrO}_2$ . However, the magnetic structure determined by neutron diffraction data refinements is not dramatically changed by the 2% Mg substitution [14]. The analysis of the  $\chi(T)$  curve of  $\text{CuCrO}_2$  and  $\text{CuCr}_{0.98}\text{Mg}_{0.02}\text{O}_2$  (inset of Fig. 8), by using the CurieWeiss law ( $\chi = \frac{C}{T - \theta_{CW}}$ ), indicates for the former a narrow T-range for the  $\chi^{-1}$  linear regime.

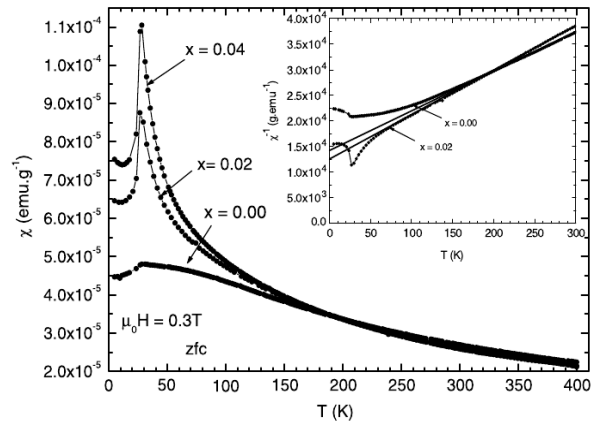


FIG. 8: T-dependent magnetic susceptibility ( $\chi$ ) for samples of the series  $\text{CuCr}_{1-x}\text{Mg}_x\text{O}_2$  ( $x$  values are labelled in the graph). Inset: T-dependent reciprocal magnetic susceptibility ( $\chi^{-1}$ ) for  $x = 0.00$  and  $x = 0.02$ ; the straight lines are for the CurieWeiss fitting curves.

Both the upward deviation of the  $\chi^{-1}(T)$  curve starting below about 200 K and the CurieWeiss constant value,  $\theta_{CW} \sim -170\text{ K}$ , indicate large antiferromagnetic fluctuations in the undoped compound. However, the effective paramagnetic moment ( $\mu_{\text{eff}}$ ) values extracted from the linear part of the  $\chi^{-1}(T)$  curves,  $\mu_{\text{eff}} \simeq 3.7 - 4.0\mu_B$ , do not significantly change with  $x$ . This value is close to the spin-only value for high spin  $\text{Cr}^{3+}$  with  $S = 3/2$ , leading to  $2[S(S+1)]^{1/2} = 3.87\mu_B$ . These values and the trend with  $x$  are in good agreement with those previously reported [11] and also with the  $\text{Cr}^{3+}$  high spin state coming from the band structure calculations.

Interestingly, the impact of the  $\text{Mg}^{2+}$  doping on the magnetic properties is accompanied by a dramatic change of the electronic properties. A large decrease of the electrical resistivity  $\rho$  values is induced,  $\rho$  decreasing at

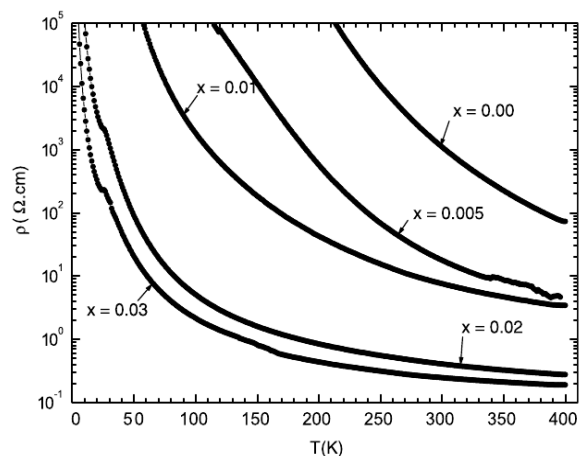


FIG. 9: T-dependent electrical resistivity ( $\rho$ ) for the series  $\text{CuCr}_{1-x}\text{Mg}_x\text{O}_2$ .

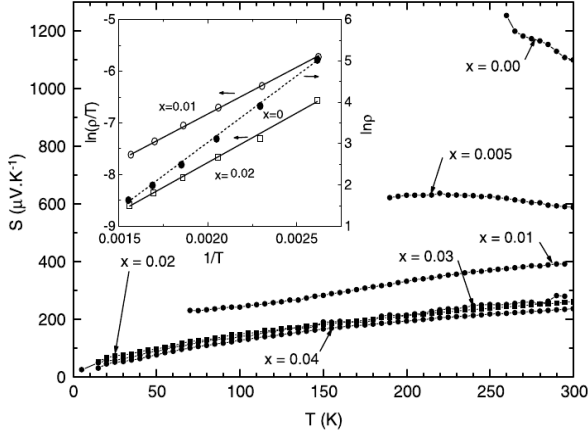


FIG. 10: T -dependent Seebeck coefficient ( $S$ ) for the series  $\text{CuCr}_{1-x}\text{Mg}_x\text{O}_2$ . Inset: inverse temperature dependence of the high temperature resistivity values for  $x = 0.00$  (right y-scale,  $\ln(\rho)$ ),  $x = 0.01$  and  $x = 0.02$  (left y-scale,  $\ln(\rho/T)$ ); the straight lines correspond to the activated behaviour ( $x = 0.00$ ) and small polaron fitting ( $x = 0.01$  and  $x = 0.02$ ).

300 K from 1 k $\Omega$  cm in  $\text{CuCrO}_2$  down to 0.3  $\Omega$  cm in  $\text{CuCr}_{0.99}\text{Mg}_{0.01}\text{O}_2$  (Fig. 9). Moreover, the Mg doping also affects the temperature dependence of the resistivity. This is illustrated by the curves shown in the inset of Fig. 10 showing the  $\rho$  data collected for  $T > 300$  K, i.e. far beyond the T region where the magnetic fluctuations might play a role. Indeed, for the undoped compound, the temperature dependence of the resistivity (in the inset of Fig. 10) is following an activated behaviour,  $\ln \rho \propto T^{-1}$ , over the temperature range where it is measurable, with an activation energy of 280 meV. In contrast, this does not hold true for the doped compound, where a small polaron behaviour,  $\ln(\rho/T) \propto T^{-1}$ , is observed in the same range of temperature with an activation energy of 170-190 meV for  $x = 0.01$  and  $x = 0.02$  in the inset of Fig. 10, as anticipated above. By further increasing the nominal content of  $\text{Mg}^{2+}$ , the  $\rho(T)$  curves keep roughly the same shape and values in agreement with the limited solubility of  $\text{Mg}^{2+}$  reached for  $x \geq 0.02$ . As already reported in Ref. [11], a kink is found at  $T_N$  for the doped samples (Fig. 9), suggesting a spin-charge coupling. This is confirmed in the case of the conducting samples by the existence of a negative magnetoresistance (MR) (Fig. 11), for  $\text{CuCr}_{0.96}\text{Mg}_{0.04}\text{O}_2$ . At 5 K, this effect reaches  $-19\%$  in 7 T [ $\% \text{MR} = 100 \times (\frac{\rho(H) - \rho(H=0)}{\rho(H=0)})$ ]. However, as T is increased, the isothermal  $\rho(H)/\rho(H=0)$  curves show that the MR magnitude follows a non-monotonic behaviour: as T increases from 5 K, the MR first decreases (curves collected at 10, 15, 25 K in Fig. 11), so that  $\text{MR} \simeq 0$  at  $T_N = 25$  K; then MR increases again just above  $T_N$  ( $T = 30$  K), and finally progressively decreases (35 K and 50 K curves). For this last T region ( $T > T_N$ ), MR is observed up to  $T \sim 70$  K (see also the  $[\rho(H=0)/\rho(H=7T)](T)$  curve for

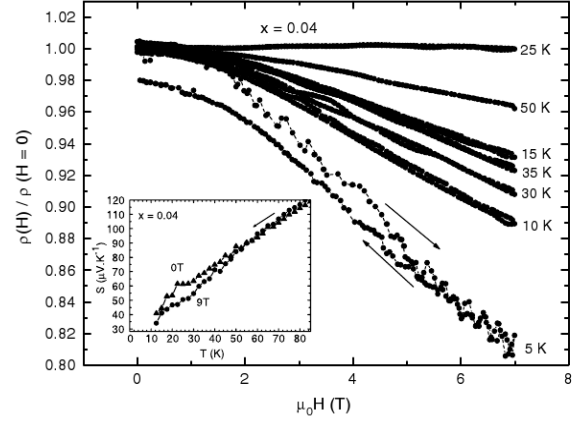


FIG. 11: Isothermal magnetic field dependent resistivity of  $\text{CuCr}_{0.96}\text{Mg}_{0.04}\text{O}_2$ . Inset: low temperature enlargement of the  $S(T)$  curves for  $\text{CuCr}_{0.96}\text{Mg}_{0.04}\text{O}_2$  collected upon cooling from 315 K in 0 T and then in 9 T.

$\text{CuCr}_{0.96}\text{Mg}_{0.04}\text{O}_2$  in the inset of Fig. 11). Thus, these compounds behave as if the application of a magnetic field above  $T_N$  reduces the spin scattering of charges leading to negative MR. This strongly resembles the conventional effect observed of spin-polarized transport in ferromagnetic conducting oxides beyond  $T_C$ . But as the magnetic ordered state is antiferromagnetic, at  $T_N$ , the setting of the long range antiferromagnetism blocks charge hopping with the corresponding  $\text{MR} = 0$ . The following negative MR for  $T < T_N$  is again due to the re-entrance of the regime due to spin-polarized transport.

The observed negative magnetoresistance strongly supports that the  $\text{Cr}^{3+}/\text{Cr}^{4+}$  mixed valence in the  $\text{CrO}_2$  layer rather than  $\text{Cu}^+/\text{Cu}^{2+}$  is responsible for the observed electrical conductivity. In that respect, the analysis of the Seebeck coefficient values gives important information. As shown in Fig. 10, the  $S_{300\text{K}}$  values decrease from 1.1 mV/K for  $\text{CuCrO}_2$  to 0.39 mV/K for  $\text{CuCr}_{0.99}\text{Mg}_{0.01}\text{O}_2$ , and then 0.26 mV/K for  $\text{CuCr}_{0.98}\text{Mg}_{0.02}\text{O}_2$ . The latter value is in good agreement with the data reported by Ono et al. [12]. For higher x values in  $\text{CuCr}_{1-x}\text{Mg}_x\text{O}_2$ ,  $S_{300\text{K}}$  saturates to about 0.25 – 0.27 mV/K. This is consistent with the limited  $\text{Mg}^{2+}$  solubility of 1% reached for nominal magnesium contents such as  $x \geq 0.02$  in  $\text{CuCr}_{1-x}\text{Mg}_x\text{O}_2$ . This explains the rather constant charge carrier concentration for  $x > 0.01$ .

This  $S$  decrease as x increases can be simply explained by using the Heikes formula,  $S = \frac{k_B}{e} [\ln(\frac{1-x}{x})]$ , where x corresponds to the  $\text{Cr}^{4+}$  density. A good agreement is found for  $\text{CuCr}_{0.96}\text{Mg}_{0.04}\text{O}_2$ :  $S_{\text{Heikes}} = 396 \mu\text{V/K}$  against  $S_{\text{exp}} = 390 \mu\text{V/K}$ . Moreover, for  $\text{CuCrO}_2$ ,  $S_{\text{exp}} = 1.1 \text{ mV/K}$  results into  $x_{\text{calc}} = 2.9 \cdot 10^{-6}$ , i.e. a very small fraction of  $\text{Cr}^{4+}$ . For larger x values, the presence of impurities revealed by X-ray diffraction precludes the analysis of the data. It must be emphasized that a charge compensation to the  $\text{Mg}^{2+}$  substitution by

creating  $\text{Cu}^{2+}$  would give the same result as a fraction of  $x(\text{Mg}^{2+})$  is creating  $x(\text{Cu}^{2+})$  corresponding to holes in a  $\text{Cu}^+$  matrix. In order to rule out one of these hypotheses, Seebeck measurements have been measured without and within magnetic field as shown for  $\text{CuCr}_{0.96}\text{Mg}_{0.04}\text{O}_2$  in the inset of Fig. 11.

Applying an external magnetic field upon cooling makes the  $S$  values decrease compared to the  $S_{H=0}(T)$  measurements. This negative magnetothermopower, which reaches a maximum at  $T_N$ , indicates a contribution of the spins to the thermopower pointing towards a spin-polarized transport in the  $\text{CrO}_2$  planes. A similar effect was found in cobaltites with isostructural  $\text{CoO}_2$  layers [32]. The existence of concomitant negative magnetoresistance and magnetothermopower in these delafossites, both related to  $T_N$ , thus supports an electronic conduction by  $\text{Cr}^{4+}$  holes in the  $\text{CrO}_2$  magnetic layer.

The most striking result of the present study is the strong impact on the magnetic and transport properties induced by low  $\text{Mg}^{2+}$  doping. It must be recalled that the  $\text{Mg}^{2+}$  solubility appears to be very limited as attested by the impurity formation already detected for the nominal composition  $\text{CuCr}_{0.99}\text{Mg}_{0.01}\text{O}_2$ . In agreement, a maximum of 1% Mg can be measured, as shown from the study of the compound of nominal composition  $\text{CuCr}_{0.98}\text{Mg}_{0.02}\text{O}_2$ . This explains the very weak  $x$ -dependence of  $\rho$ ,  $S$  and  $\chi$  observed for  $x \geq 0.02$  in  $\text{CuCr}_{1-x}\text{Mg}_x\text{O}_2$ .

#### IV. DISCUSSION AND CONCLUDING REMARKS

The present study reveals that the  $\text{Mg}^{2+}$  solubility in the  $\text{CuCr}_{1-x}\text{Mg}_x\text{O}_2$  delafossite is limited to 1%. As shown by the electronic band structure, in the  $\text{CuCrO}_2$  starting material, the main contributions, at the valence band maximum, are given by the  $\text{Cr}^{3+} t_{2g}$  orbitals, the  $\text{Cu } 3d$  states lying much deeper in energy. As a result, in the absence of doping, the compound is semi-conducting. This is consistent with the large Seebeck coefficient at room temperature,  $S = 1.1$  mV/K. In contrast to  $\text{PdCoO}_2$ , for which the lack of  $\text{Co}^{3+}$  contribution of the  $\text{CoO}_2$  layer to the electronic states gives a strong 2D character to these states mainly driven by the  $\text{Pd}^+$  species, the  $\text{CrO}_2$  contribution creates 3D electronic states ensuring a strong interlayer coupling. The latter is attested by the long range non-commensurate antiferromagnetism of  $\text{CuCrO}_2$  [14]. The spin-polarized calculations point towards a band gap between spin-up and spin-down with  $3\mu_B$  per  $\text{Cr}^{3+}$ . The discrepancies between our  $\rho$  and  $S$  data and those of previous studies for the starting  $\text{CuCrO}_2$  oxide reflect its great sensitivity

to doping. This study demonstrates that complete sets of synthesis and structural characterizations are needed to exclude the presence of non-stoichiometry phenomena that could be very tiny. For instance, the larger  $S$  values at 300 K, indicating smaller hole concentration, point towards the more stoichiometric character of our samples as compared to those of Ref. [11]. In addition, the presence of impurities, detected even for the  $x = 0.01$  compound, shows that the measurements made in previous studies for samples containing probably some impurities could not easily be trusted. As far as electrical transport is concerned, these impurities could act as parallel circuits, thus rendering the interpretations difficult.

Starting from the electronic structure of  $\text{CuCrO}_2$ , hole doping ( $\text{Cr}^{4+}$ ) in the  $\text{Cr}^{3+}$  matrix would create charge carrier delocalisation in a spin-polarized media. This scenario based on a transport made on the  $\text{CrO}$  network rather than on the  $\text{Cu}$  one is confirmed by the bump observed at  $T_N$  on the  $\rho(T)$  curves for  $x \geq 0.02$ , the negative magnetothermopower and magnetoresistance. For the latter, the spin scattering reduction induced by the application of a magnetic field is responsible for the negative MR observed above  $T_N$ . At  $T_N$ , the antiferromagnetic setting blocks the spin scattering so that magnetic field application has no longer an effect on the electrical resistivity (in Fig. 11 and within 7 T,  $\text{MR} = 0$  at  $T_N = 25$  K to be compared to  $\text{MR} = -9\%$  at 30 K). In that respect, the re-entrance of the MR for  $T < T_N$  might correspond to remaining disordered spin regions which locally allow some magnetic moment reorientation under the application of a magnetic field.

One of the major results of this study is that only 1%  $\text{Mg}^{2+}$  substitution for  $\text{Cr}^{3+}$ , formally creating 1% of  $\text{Cr}^{4+}$ , is sufficient to drastically modify the electronic properties. Such an effect can be compared to the doping effects in transparent conducting oxides as  $\text{Sn}^{4+}$ -doped  $\text{In}_2\text{O}_3$  (ITO). However, the magnetism of the high spin states of chromium trivalent and tetravalent cations in  $\text{CuCrO}_2$  is responsible for spin polarization. Accordingly, the drastic decrease of the electrical resistivity induced by the substitution is reinforcing the magnetic ordering via the coupling between holes and spins. This explains the higher  $T_N$  value observed for Mg-substituted  $\text{CuCrO}_2$  [11,14].

#### V. ACKNOWLEDGMENTS

We gratefully acknowledge many useful discussions with T. Kopp, V. Hardy, Ch. Simon and W. C. Sheets. This work was supported by the Deutsche Forschungsgemeinschaft through SFB 484.

<sup>1</sup> J.G. Bednorz, K.A. Müller, Z. Phys. B **64**, 189 (1986).

<sup>2</sup> K. Mitzushima, et al., Mat. Res. Bull. **15**, 783 (1980).



- <sup>3</sup> I. Terasaki, Y. Sasago, K. Uchinokura, Phys. Rev. B **56**, R 12685 (1997).
- <sup>4</sup> K. Takada, et al., Nature **422**, 53 (2003).
- <sup>5</sup> M. Von Jansen, R. Hoppe, Z. Anorg. Allg. Chem. **408**, 104 (1974).
- <sup>6</sup> D.J. Singh, Phys. Rev. B **61**, 13397 (2000).
- <sup>7</sup> K. Takeda, et al., J. Phys. Soc. Japan **63**, 2017 (1994).
- <sup>8</sup> T. Kimura, J. C. Lashley, and A. P. Ramirez, Phys. Rev. B **73**, 220401(R) (2006).
- <sup>9</sup> A. Pabst, Am. Mineral. **23**, 175 (1938).
- <sup>10</sup> F. Ye, et al., Phys. Rev. B **73**, 220404 (2006).
- <sup>11</sup> T. Okuda, et al., Phys. Rev. B **72**, 144403 (2005); T. Okuda, et al., Phys. Rev. B **77**, 134423 (2008).
- <sup>12</sup> Y. Ono, K. Satoh, T. Nozaki, and T. Kajitani, Jap. J. Appl. Phys. **46**, 1071 (2007).
- <sup>13</sup> H. Kadowaki, H. Kikuchi, Y. Ajiro, J. Phys.: Condens. Matter **2**, 4485 (1990).
- <sup>14</sup> M. Poienar, et al., Phys. Rev. B **79**, 014412 (2009).
- <sup>15</sup> S. Seki, Y. Onose, and Y. Tokura, Phys. Rev. Lett. **101**, 067204 (2008).
- <sup>16</sup> J.P. Perdew, K. Burke, M. Ernzerhof, Phys. Rev. Lett. **77**, 3865 (1996).
- <sup>17</sup> J.P. Perdew, Y. Wang, Phys. Rev. B **45**, 13244 (1992).
- <sup>18</sup> A. R. Williams, J. Kübler, and C. D. Gelatt, Jr., Phys. Rev. B **19**, 6094 (1979).
- <sup>19</sup> V. Eyert, Int. J. Quantum Chem. **77**, 1007 (2000).
- <sup>20</sup> V. Eyert, *The Augmented Spherical Wave Method – A Comprehensive Treatment*, Lect. Notes Phys. **719** (Springer, Berlin Heidelberg 2007).
- <sup>21</sup> V. Eyert and K.-H. Höck, Phys. Rev. B **57**, 12727 (1998).
- <sup>22</sup> V. Eyert, J. Comp. Phys. **124**, 271 (1996).
- <sup>23</sup> P. E. Blöchl, O. Jepsen, and O. K. Andersen, Phys. Rev. B **49**, 16223 (1994).
- <sup>24</sup> V. Eyert, unpublished
- <sup>25</sup> M. S. Methfessel, Phys. Rev. B **38**, 1537 (1988).
- <sup>26</sup> O. Crottaz, F. Kubel, H. Schmid, J. Solid State Chem. **122**, 247 (1996).
- <sup>27</sup> V. R. Galakhov, A. I. Poteryaev, E. Z. Kurmaev, V. I. Anisimov, S. Bartkowski, M. Neumann, Z. W. Lu, B. M. Klein, and T.-R. Zhao, Phys. Rev. B **56**, 4584 (1997).
- <sup>28</sup> K. P. Ong, K. Bai, P. Blaha, and P. Wu, Chem. Mater. **19**, 634 (2007).
- <sup>29</sup> V. Eyert, R. Frésard, and A. Maignan, Phys. Rev. B **78**, 052402 (2008).
- <sup>30</sup> V. Eyert, R. Frésard, and A. Maignan, Chem. Mat. **20**, 2370 (2008).
- <sup>31</sup> D. J. Singh, Phys. Rev. B **76**, 085110 (2007).
- <sup>32</sup> P. Limelette, et al., Phys. Rev. Lett. **97**, 046601 (2006).